AD

AD-E404 350

Technical Report ARWSE-TR-19003

YAWSONDE SOLAR SENSOR ASSESSMENT

Stephan Zuber
James Hitscherich
Andrew Lansey

February 2022

U.S. ARMY COMBAT CAPABILITIES DEVELOPMENT
COMMAND ARMAMENTS CENTER

Weapons and Software Engineering Center

Picatinny Arsenal, New Jersey

The views, opinions, and/or findings contained in this report are those of the author(s) and should not be construed as an official Department of the Army position, policy, or decision, unless so designated by other documentation.

The citation in this report of the names of commercial firms or commercially available products or services does not constitute official endorsement by or approval of the U.S. Government.

Destroy by any means possible to prevent disclosure of contents or reconstruction of the document. Do not return to the originator.

REPORT DOCUMENTATION PAGE

PLEASE DO NOT RETURN YOUR FORM TO THE ABOVE ORGANIZATION.

1. REPORT DATE	2. REPORT TYPE	3. DATES COVERED	
		START DATE	END DATE
February 2022	Final		

4. TITLE AND SUBTITLE
Yawsonde Solar Sensor Assessment

5a. CONTRACT NUMBER	5b. GRANT NUMBER	5c. PROGRAM ELEMENT NUMBER
5d. PROJECT NUMBER	5e. TASK NUMBER	5f. WORK UNIT NUMBER

6. AUTHOR(S)
Stephan Zuber, James Hitscherich, and Andrew Lansey

7. PERFORMING ORGANIZATION NAME(S) AND ADDRESS(ES)	8. PERFORMING ORGANIZATION REPORT NUMBER
U.S. Army DEVCOM AC, WSEC Fire Control Systems and Technology Directorate Optics Metrology Lab, Small Arms Fire Control Division (FCDD-ACW-FN) Picatinny Arsenal, NJ 07806-5000	N\A

9. SPONSORING/MONITORING AGENCY NAME(S) AND ADDRESS(ES)	10. SPONSOR/MONITOR'S ACRONYM(S)	11. SPONSOR/MONITOR'S REPORT NUMBER(S)
U.S. Army DEVCOM AC, ESIC Knowledge & Process Management Office (FCDD-ACE-K) Picatinny Arsenal, NJ 07806-5000		Technical Report ARWSE-TR-19003

12. DISTRIBUTION/AVAILABILITY STATEMENT
Approved for public release; distribution is unlimited.

13. SUPPLEMENTARY NOTES

14. ABSTRACT
The Yawsonde solar sensor is a photosensitive waveguide used to determine the flight attitude of a projectile when it is moving towards, at, and after its apogee. This sensor design has been assessed since the 70s, and different shapes and configurations have been analyzed, see references for past resources. The current sensor design used on the family of 155-mm projectiles used by the U.S. Army is now under re-assessment. Currently, the complexity of the design, its ability to be manufactured, and the high cost associated with such are primary factors causing this new review. A tasker was made if the optical metrology team within the Small Arms Fire Control division, Weapons Systems and Engineering Center directorate, at the U.S. Army Combat Capabilities Development Command Armaments Center, Picatinny Arsenal, NJ, could perform a preliminary review on potential lower cost replacements for the sensor assembly. This paper describes the current fielded sensor design and several potential options that may lead to reducing the component costs and complexities. Several modeling experiments took place to show current optical performance for each of the options considered in this initial review.

15. SUBJECT TERMS
Optic Fire control 155 mm Solar sensor Yawsonde Attitude

16. SECURITY CLASSIFICATION OF:			17. LIMITATION OF ABSTRACT	18. NUMBER OF PAGES
a. REPORT	b. ABSTRACT	c. THIS PAGE		
U	U	U	SAR	25

19a. NAME OF RESPONSIBLE PERSON	19b. PHONE NUMBER (Include area code)
Stephan Zuber	(973) 724-4130

Standard Form 298 (REV. 5/2020)
Prescribed by ANSI Std. Z39.18

CONTENTS

FIGURES

FIGURES
(continued)

INTRODUCTION

The Yawsonde solar sensor is a photosensitive waveguide used to determine flight attitude of a projectile when it's moving toward, at, and after its apogee. The attitude can be described as the inclination of the three axes (position) of the projectile in respect to a relative wind direction or its position relative to the earth—simply put, the yaw and rotation of the projectile. As a military application, this type of sensor can be integrated into a munitions fuze or guidance system in order to measure a relative intensity of light coming from the sun based on its position and orientation in flight. As the projectile reaches apogee, the intensity would be expected to reach a maximum value given the reduction in atmospheric conditions (barometric pressure), which attenuate the incoming or incident light (visible, near infrared [NIR]). This sensor design has been assessed since the 1970s, and different shapes and configurations have been analyzed, see references for past resources. The current sensor design used on the family of 155-mm projectiles used by the U.S. Army is now under re-assessment. Currently, the complexity of the design, its ability to be manufactured, and the high cost associated with such are the primary factors causing this new review. A tasker was made if the optical metrology team within the Small Arms Fire Control (SAFC) division, Weapons Systems and Engineering Center (WSEC) directorate, at the Combat Capabilities Development Command (DEVCOM) Armaments Center (AC), Picatinny Arsenal, NJ, could perform a preliminary review on potential lower cost replacements for the sensor assembly. This paper describes the current fielded sensor design, and several potential options that may lead to reducing the component costs and complexities. Several modeling experiments took place to show current optical performance for each of the options considered in this initial review. Figure 1 depicts the solar sensor assembly when installed on a facsimile 155-mm fuze. The criteria to follow as guidelines in this effort include the following:

- Shock survivability - Up to 20 kg, it must survive projectile setback.
- Spin - Must survive centrifugal forces of 300 Hz at a 3-in. radius.
- Profile - Mimics the current sensor (0.2 x 0 x 0.716 in. with 0 x 0.63-in. rounded corners) for backwards compatibility.
- Depth - Mimic current 0.366-in. depth but can be slightly greater than 0.5 in.
- Try to mimic field of view (FOV) of current reflector assembly.
- Photodiode - Use the Luna PDB-C607-2 or Marktech MTD3610D3 model.
- Manufacturing cost and lead time: Target would be $100/ea. or less in quantities of 20 to 100 and have a build time of less than 1 to 2 months.

Figure 1
Yawsonde solar sensor assembly placement on a 155-mm fuze

TESTS, DESCRIPTIONS, AND RESULTS

Current Reflector and Assembly Design

The current sensor design incorporates three primary optical components that include two reflectors that are symmetrically opposed to one another, and a Luna silicon photodiode (model PDB-C607-2) that was treated as a single 1 x 1 rectangular pixel array. The remaining components that make up the rest of the sensor assembly are stainless steel pins that align and hold the assembly together, a polycarbonate cup to house the photodiode, an aluminum exterior housing, epoxy, and optically invisible adhesive. The precision and complexity of manufacturing and assembling these materials and overall configuration come at a high cost and long lead time to manufacture. The very small size, tight tolerances, and the shape and material the reflectors comprise of play the largest factors in these issues. The reflectors themselves are nickel plated brass to obtain a functional reflection, and the shape requires additional constraints in order to mill, machine or cast. Figure 2 provides a cutaway view of the entire solar assembly.

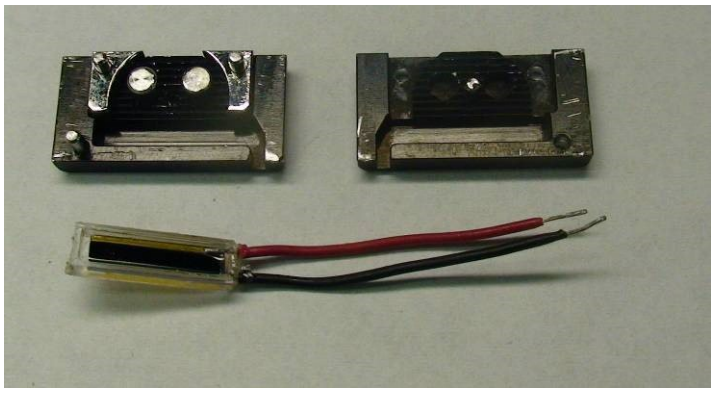

Figure 2
Photograph of Yawsonde solar sensor assembly

Current Reflector and Assembly Zemax Modeling

To begin to fully understand the optical performance of the current design, a primary assumption had to be made regarding the photodiode. Rather than an array of pixels, the diode was treated as 1 x 1 pixel or a single pixel. This assumption simplified the preliminary results such that any hit on the diode or herein referred to as the detector counted only a hit or miss of an incoming photon or ray. This removed any considerations of dealing with variations in incident photon energy or energy loss in a reflection event. The method of characterizing the sensor design and subsequent options in design changes used the Zemax OpticStudio modeling software (ref. 1). This program allows the development of an emitter or source to match the general size and output of the sun in normal daylight conditions relative to the position of the earth. To start, the CAD or ProE file was imported directly into software as a .stp file.

The source (i.e., the Sun) was then preconfigured to have an arc length of 30 arcminutes (arcmin) or 9.3 milliradians (mrad), simulating the angular subtense of the Sun relative to the Earth and using an output based on the F, d, and C standard spectral lines. These lines are .486, .588 and .656 microns. The source was then placed at a distance such that its focal range was roughly at infinity relative to the sensor assembly. The source and sensor were then aligned with each other such that the primary ray trace was orthogonal to the photodiode through the opening slit of the assembly. A detector plane was then overlaid across the top of the photodiode and its holding cup. This made the assumption that the holding cup had no optical attenuation effects between the source and the diode. For a random source baseline, 10 total rays were used and analyzed for each

model in this report for each design and situation. Also note that all reflecting surfaces were designated as mirrors (protected aluminum) in the software which assumed perfect optical conditions regarding material.

No Angle of Rotation – Direct Orthogonal Emitter

Figure 3 presents the first model showing the placement where all the incident energy of the ray trace reflected off of the alignment pin and blocked the rays from reaching the detector plane. This configuration is referred to the source as having 0 deg of rotation from the central axis of the assembly. Figure 4 presents a mock version of the sensor assembly without the pins, which shows all 10 rays reaching the detector with a total energy of 6.05 W/cm^2. Figures 5 and 6 provide additional confirmation that any rays placed between the alignment pins would fully pass into the detector. These three source positons are the 1st, 2nd, and 3rd source positions used in all the design assessments. The real assembly showed that the direct orthogonal path impedes all photons that are incident into the center pin. See table 1 for complete details on which positons, designs, and other considerations that affected the readout at the detector plane.

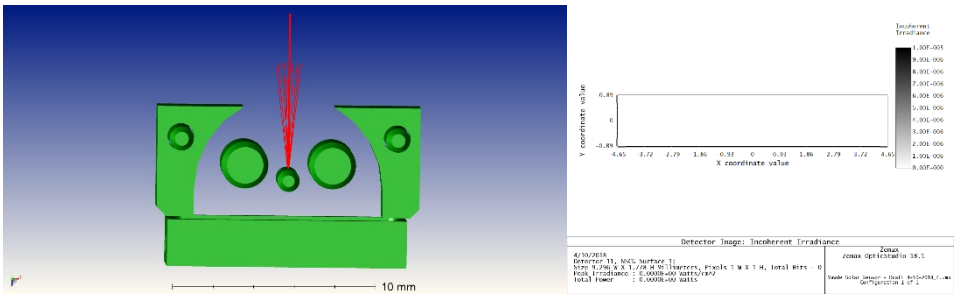

Figure 3
Current design, with pins, 0-deg critical angle

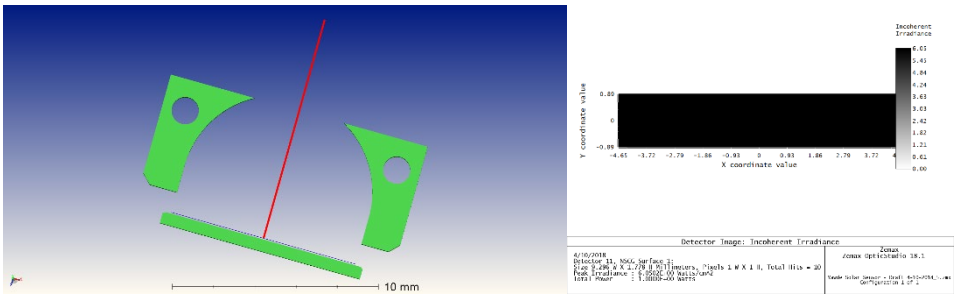

Figure 4
Current design, without pins, 0-deg critical angle

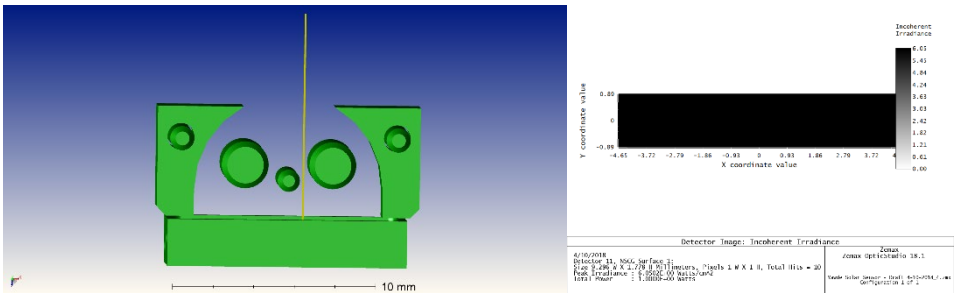

Figure 5
Current design, with pins, -0-deg critical angle

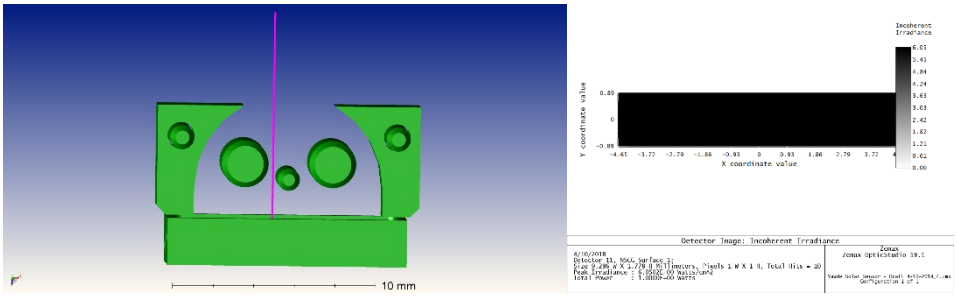

Current design, with pins, +0-deg critical angle

Table 1
Detector readouts for the current, and tapered style design concepts for each emitter angle

	1x1 Photodiode detector	**Emitter angle, (-) 0**	
Sensor design	Incoherent irradiance, maximum (W/cm2)	Incoherent irradiance, nominal	Number of hits
Current w/pins *	6.05	3.63	10
Current w/o pins *	6.05	3.63	10
Aluminum w/pins	>/= Current		
Aluminum w/o pins			
Tapered reflectors w/pins	6.05	3.63	10
Tapered reflectors w/o pins	6.05	3.63	10
Compound tapered reflectors w/pins	6.05	3.63	10
Compound tapered reflectors w/o pins	6.05	3.63	10
	1x1 Photodiode detector	**Emitter angle, (+) 0**	
Sensor design	Incoherent irradiance, maximum (W/cm2)	Incoherent irradiance, nominal	Number of hits
Current w/pins *	6.05	3.63	10
Current w/o pins *	6.05	3.63	10
Aluminum w/pins	>/= Current		
Aluminum w/o pins			
Tapered reflectors w/pins	6.05	3.63	10

Table 1
(continued)

Tapered reflectors w/o pins	6.05	3.63	10
Compound tapered reflectors w/pins	6.05	3.63	10
Compound tapered reflectors w/o pins	6.05	3.63	10
	1x1 Photodiode detector	**Emitter angle, 0**	
Sensor design	Incoherent irradiance, maximum	Incoherent irradiance, nominal	Number of hits
Current w/pins *	0	0	0
Current w/o pins *	6.05	3.63	10
Aluminum w/pins	>/= Current		
Aluminum w/o pins			
Tapered reflectors w/pins	0	0	0
Tapered reflectors w/o pins	0	0	0
Compound tapered reflectors w/pins	0	0	0
Compound tapered reflectors w/o pins	0	0	0
	1x1 Photodiode detector	**Emitter angle, -69.0**	
Sensor design	Incoherent irradiance, maximum	Incoherent irradiance, nominal	Number of hits
Current w/pins *	6.05	3.63	10
Current w/o pins *	6.05	3.63	10
Aluminum w/pins	>/= Current		
Aluminum w/o pins			
Tapered reflectors w/pins	0	0	0
Tapered reflectors w/o pins	6.05	3.63	10
Compound tapered reflectors w/pins	0	0	0
Compound tapered reflectors w/o pins	6.05	3.63	10
	1x1 Photodiode detector	**Emitter angle, +69.0**	
Sensor design	Incoherent irradiance, maximum	Incoherent irradiance, nominal	Number of hits
Current w/pins *	6.05	3.63	10
Current w/o pins *	6.05	3.63	10
Aluminum w/pins	>/= Current		
Aluminum w/o pins			
Tapered reflectors w/pins	0	0	0
Tapered reflectors w/o pins	6.05	3.63	10
Compound tapered reflectors w/pins	0	0	0
Compound tapered reflectors w/o pins	6.05	3.63	10

Table 1
(continued)

	1x1 Photodiode detector	**Emitter angle, -81.5**	
Sensor Design	Incoherent irradiance, maximum	Incoherent irradiance, nominal	Number of hits
Current w/pins *	6.05	3.63	10
Current w/o pins *	6.05	3.63	10
Aluminum w/pins	>/= Current		
Aluminum w/o pins			
Tapered reflectors w/pins	0.605	0.363	1
Tapered reflectors w/o pins	5.4452	3.27	9
Compound tapered reflectors w/pins	0	0	0
Compound tapered reflectors w/o pins	6.05	3.63	10
	1x1 Photodiode detector	**Emitter angle, +81.5**	
Sensor design	Incoherent irradiance, maximum (W/cm2)	Incoherent irradiance, nominal	Number of hits
Current w/pins *	6.05	3.63	10
Current w/o pins *	6.05	3.63	10
Aluminum w/pins	>/= Current		
Aluminum w/o pins			
Tapered reflectors w/pins	1.82E+00	1.09	3
Tapered reflectors w/o pins	5.4452	3.27	9
Compound tapered reflectors w/pins	0	0	0
Compound tapered reflectors w/o pins	6.05	3.63	10

Large Angle Rotation – Rotated Emitter

To model the sensor as the source traverses the slit opening, a large angle of source rotation was used. The empirical value used was 69.0-deg, which was the 4th (positive) and 5th (negative) source positons used to assess the reflection performance of the reflectors within the assembly. In these source positions, the upper curvature of the interior of the reflectors could be examined. At these source positions, the rays were shown to pass around the alignment pins and still reach the detector. Figures 7 and 8 present the model outputs for both the real and mock pinless assemblies using the positive angle. Figures 9 and 10 present the model outputs for both the real and mock pinless assemblies using the negative angle. At these angles, all the incident photons entering the slit impinged onto the detector for both pin and pinless designs, see table 1.

\

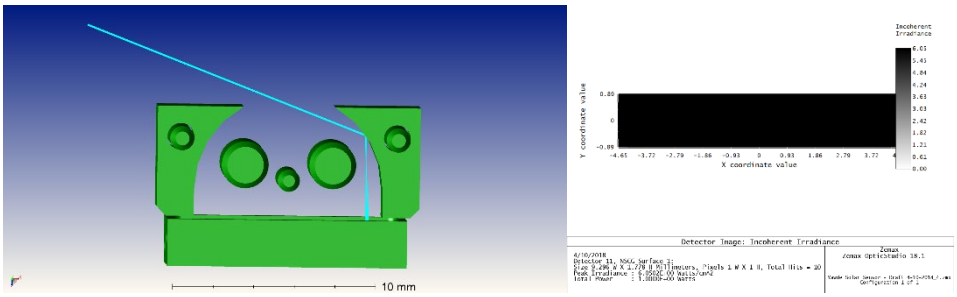

Figure 7
Current design, with pins, +69.0-deg critical angle

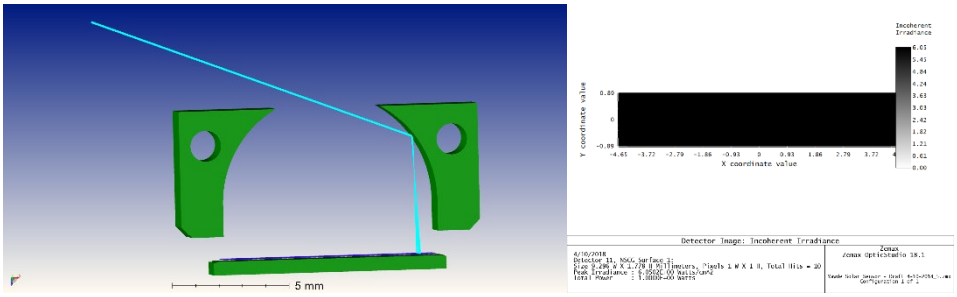

Figure 8
Current design, without pins, +69.0-deg critical angle

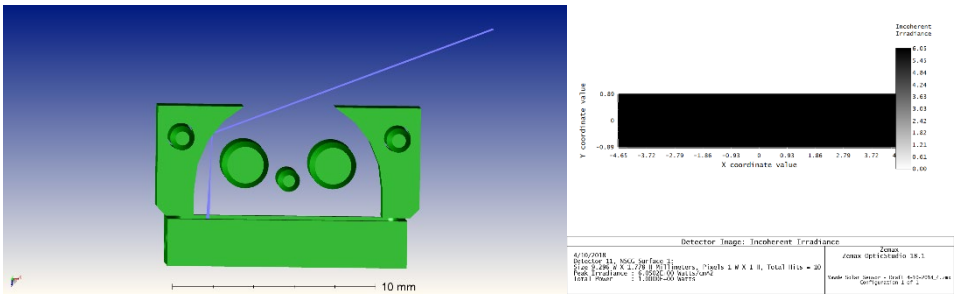

Figure 9
Current design, with pins, -69.0-deg critical angle

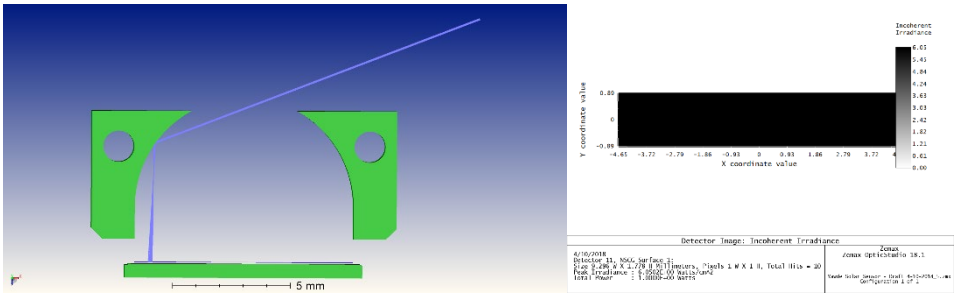

Figure 10
Current design, without pins, -69.0-deg critical angle

Critical Angle of Rotation – Edge Emitter

At this point, when the source's primary rays no longer enter the slit opening, the critical angles were empirically and mathematically determined. This angle of source rotation was at the +/-81.5-deg positions and corresponded to the 6th (positive) and 7th (negative) placement to assess reflector performance. This angle is the critical angle at which any further rotation would result in no rays entering the slit. At this position, the rays also reflect off of the interior of the reflectors in order to reach the detector plane. Figures 11 and 12 present the model outputs for both the real and mock pinless assemblies using the positive critical angle. Figures 13 and 14 present the model outputs for both the real and mock pinless assembles using the negative critical angle. As was the case with the 60-deg rotation, all incident photons entering the slit reached the detector for both design considerations, see table 1.

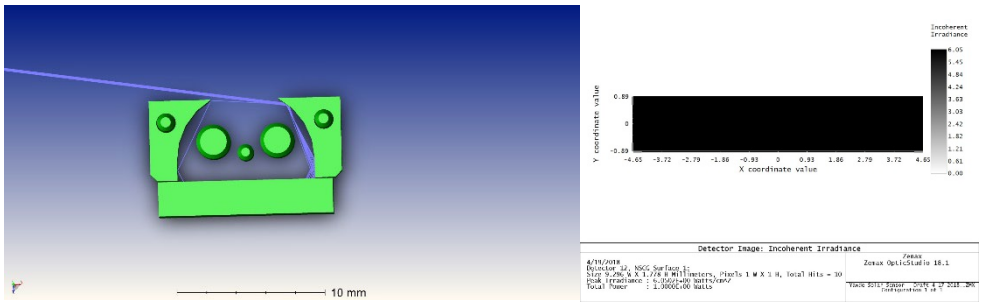

Figure 11
Current design, with pins, +81.5-deg critical angle

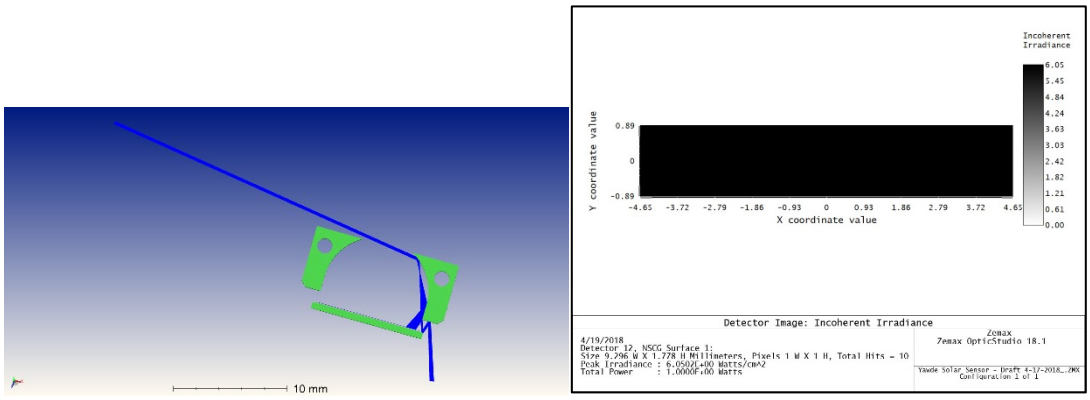

Figure 12
Current design, without pins, +81.5-deg critical angle

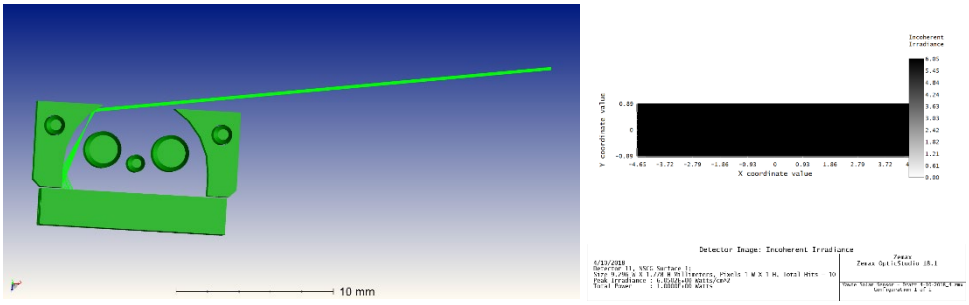

Figure 13
Current design, with pins, -81.5-deg critical angle

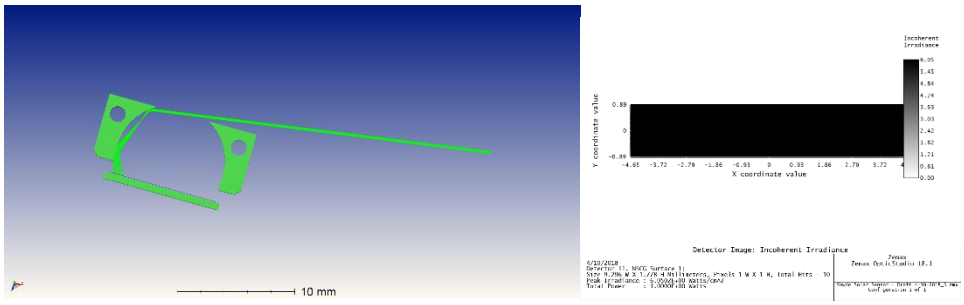

Figure 14
Current design, no pins, -81.5-deg critical angle

Reflector and Assembly Redesign, Concept 1, Material Change

Upon initial review of the design, materials, and function of the solar sensor, a first order solution was readily apparent. The reflectors are made of nickel plated brass. Nickel has a nominal reflectance value of approximately 67% for a wavelength of 588 nm (ref. 2). This efficiency of reflecting roughly 2/3 of the incident light reaching the surface retains approximately the same value through the visible and NIR wavelengths, specifically the nominal 950-nm range that the photodiode is optimally detecting.

Aluminum, polished aluminum, and/or optical grade aluminum can produce reflectance values of 91 to 93% (ref. 2). Using any of these in place of the nickel plated brass would result not only in an optically better reflector but also be cheaper in raw material costs and in mill, machining, and manufacturing costs. This is the easiest redesign solution but may result in a cost and time savings not large enough to justify the change. Further assessment into current market costs would need to be reviewed to assure the actual level of available savings.

Reflector and Assembly Redesign, Concept 2, Tapered Reflector A

The second potential option that was reviewed for a redesigned reflector was the use of simplifying the interior shape of the reflectors themselves. In this configuration, the upper opening of the slit was connected directly to the lower end of the reflector through a flat straight interface rather than the current curved edge. This concept was thought to reduce machining costs and maintain reflection around the pins. However, in the first attempts, this design appears to be incompatible with the current diameter of the pins and/or the width of the reflectors. Reducing the size of one or both components may result in a comparable light transfer to the detector. This notion is reinforced in a later design option (tapered cone), which proves this may be a viable option if resizing is applied. Figure 15 provides the design change to the reflectors using tapered style A. Figures 16, 17, 18, and 19 provide the additional angle perspectives for the taper style A design for reference. The overall detector readouts for each incident angle and configuration can be found in table 1.

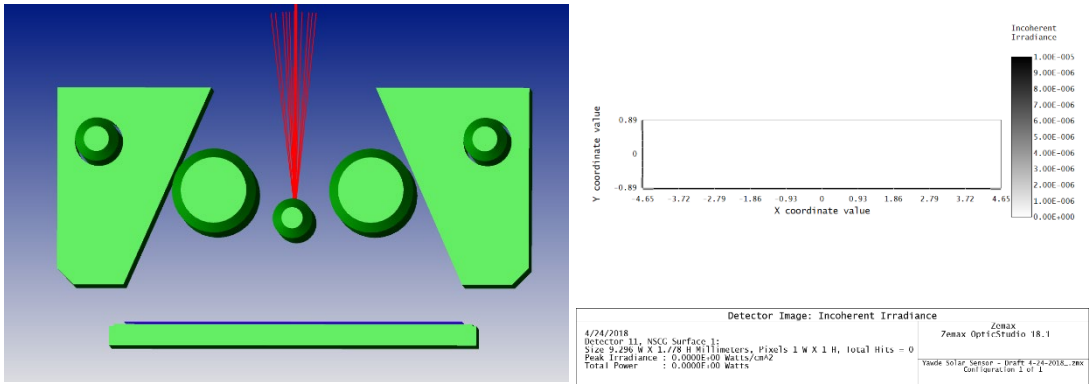

Figure 15
Tapered reflector style A, 0-deg incident rays on shaded model (left), and detector output (right)

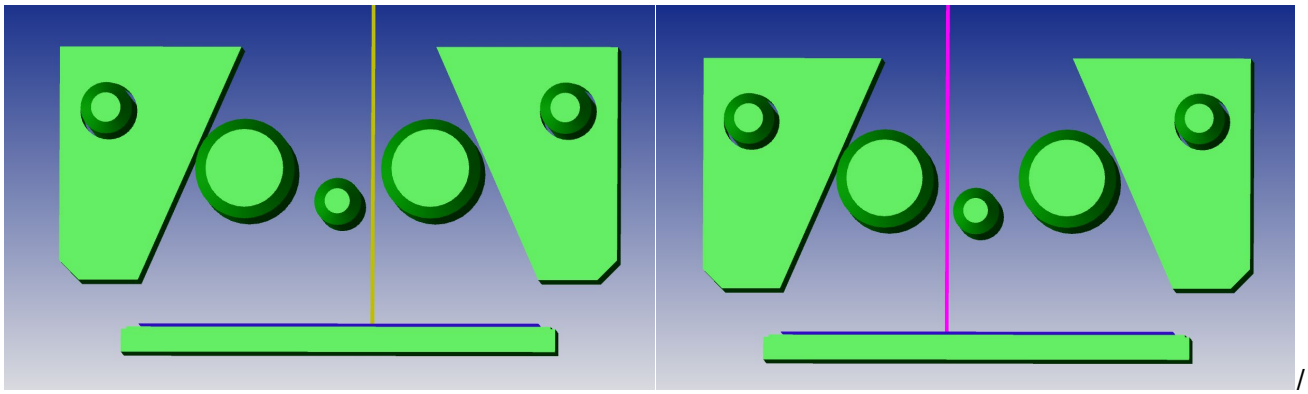

/

Figure 16
Tapered reflector style A, off axis 0-deg incident rays on positive (left), negative (right)

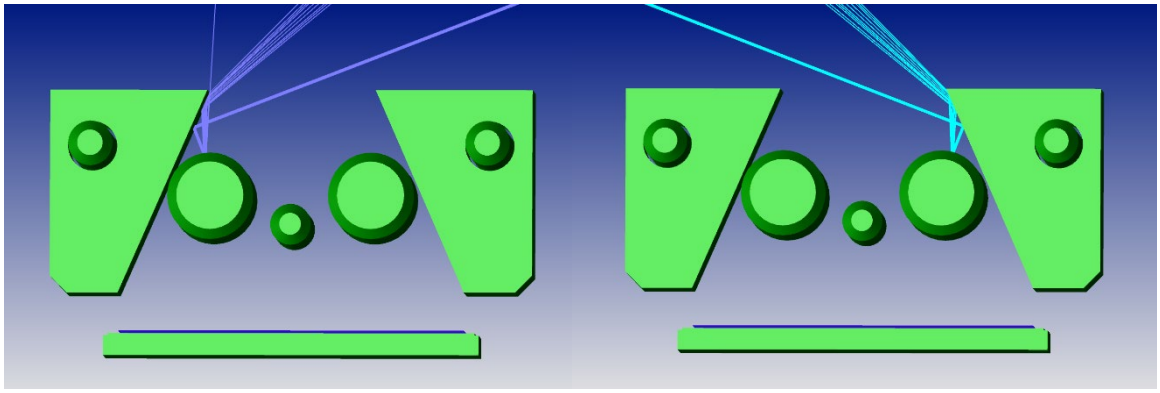

Figure 17
Tapered reflector style A, 69-deg incident rays; positive (left), negative (right)

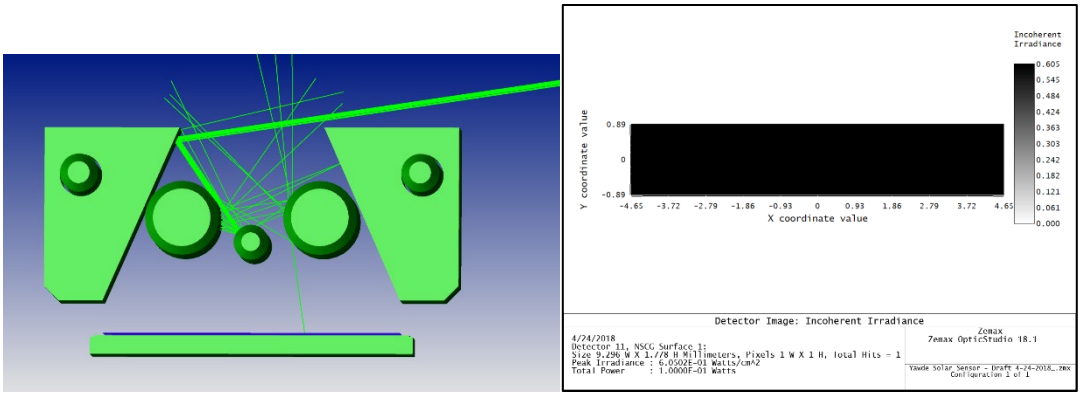

Figure 18
Tapered reflector style A, -81.5-deg incident rays; shaded model (left), detector output (right)

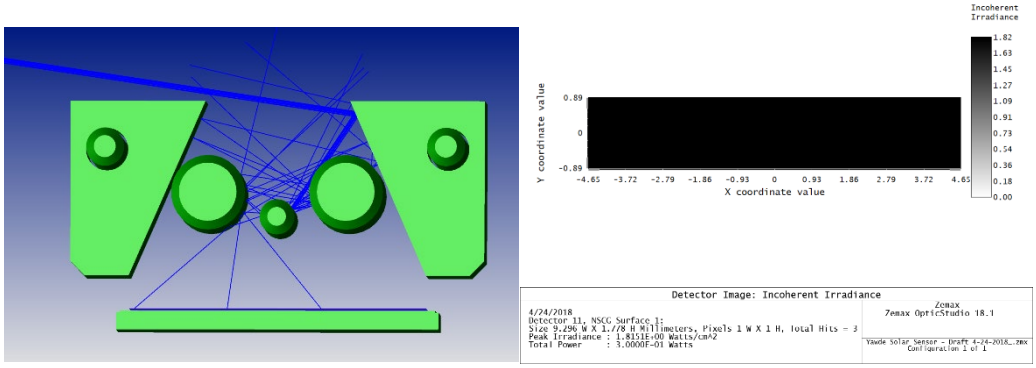

Figure 19
Tapered reflector style A, +81.5-deg incident rays; shaded model (left), detector output (right)

In addition to using the actual assembly design, another mock version using a pinless assembly was also modeled for additional information; but for the tapered designs, the small center alignment pin was left in place. The results of this model are also included in table 1 for reference.

Reflector and Assembly Redesign, Concept 3, Tapered Reflector B

The third design consideration was another method of tapering the internal reflectors but in a different method than style A. In this case, the inner slit was connected by a flat straight taper which ends with the actual end of the curvature rather than ending at the bottom of the reflector. This design concept can be seen in figure 20. In this design, additional space was allotted between the pins and the reflector, but overall it had poor performance at nearly every incident angle. This concept would also cost slightly more to mill/machine in respect to the style A taper. These two conditions lower the viability versus the previous taper style and the option of changing the reflecting material to aluminum. Although increasing the distance between the reflector tapered surface and the pins may result in an equivalent performance to the current design, this concept is not seen as a viable option worth pursuing. Figure 21 provides additional perspective on the model for the large 69 and 81.5-deg rotation angles. Refer back to table 1 for the comparative detector data for this design against the other options using the same general sensor assembly.

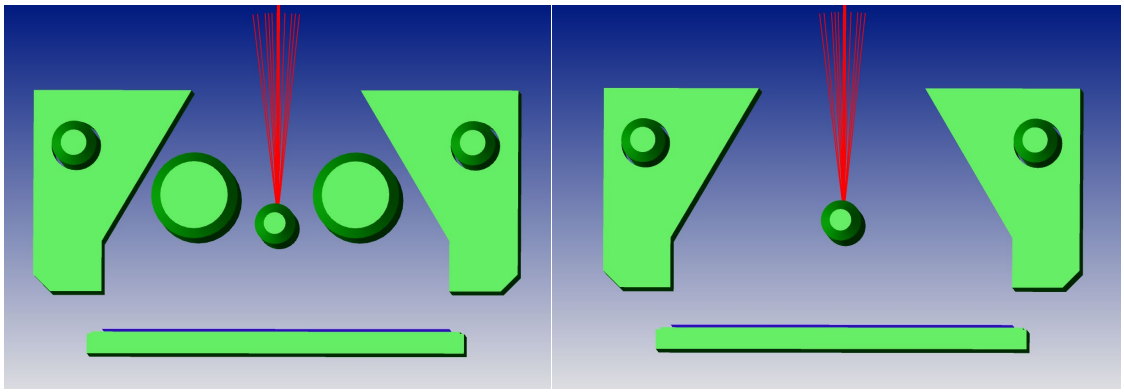

Figure 20
Tapered reflector style B, 0-deg incident rays on shaded model; with pins (left), without pins (right)

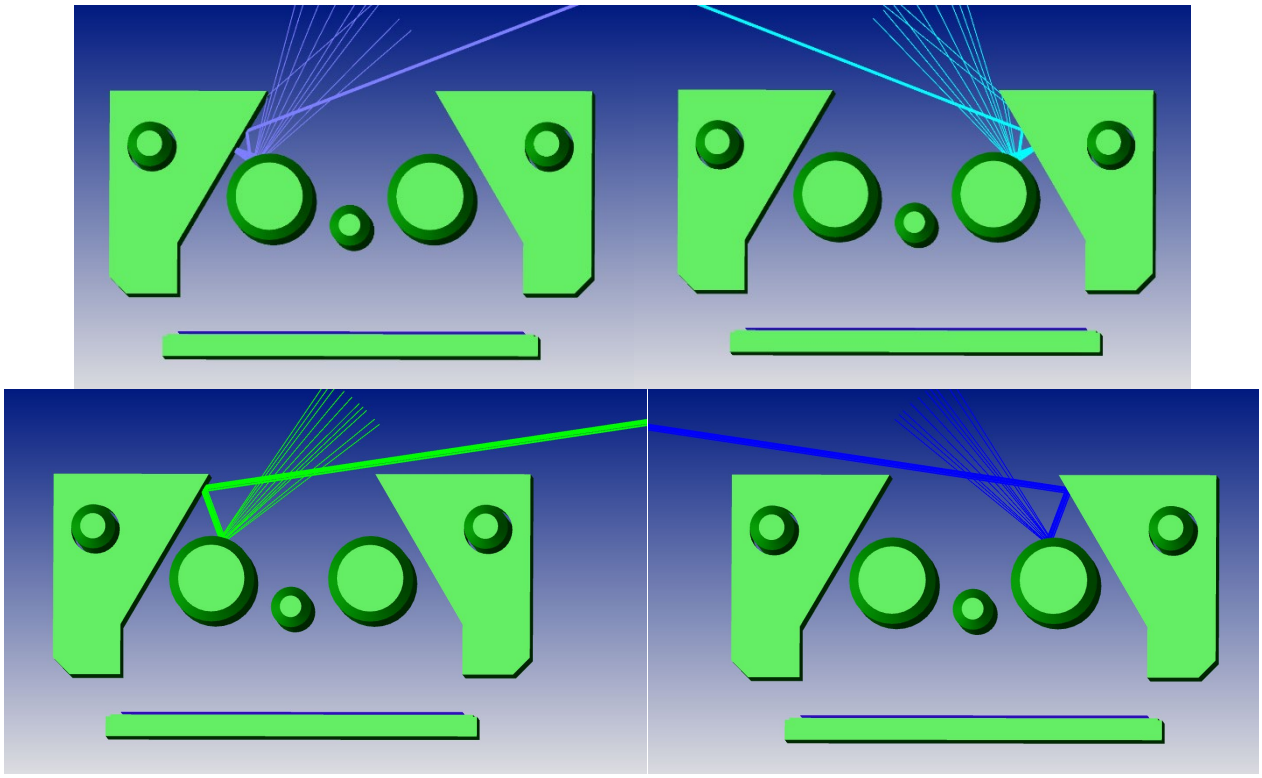

Figure 21
Tapered reflector style B, +/-69-deg angles (top left and right), +/-81.5-deg angles (bottom left and right)

Reflector and Assembly Redesign, Concept 4, Cylindrical Lens

The fourth design option that was reviewed for the Yawsonde solar sensor was the complete removal of the current reflectors and total replacement with a commercially available cylindrical lens. In this case, a ThorLabs LJ1942L1 N-BK-7 glass cylindrical lens was used. This concept can be mounted to an exterior holding frame using an optical quality adhesive such as Norland 61 (NOA-61) which is UV cured and hardened in seconds, and is optically transparent. The general concept can be seen in figure 22. The detector plane, which would be the photodiode and holding cup, is located on the flat plane of the asymmetrical lens. Using the same source (the sun) and incident angles, the design is equivalent in guiding the photons into the detector in the same manner as the current

design. This excludes, however, the critical angles at the extremes of +/-81.5 deg. For this design the critical angle is between the 69 and 81.5-deg increment and was not specifically determined at this stage of modeling. This is a small limitation that is inherent to this design and is not easily overcome without over complicating the concept. The cost per unit is listed to be $54.06 for quantities under 10.

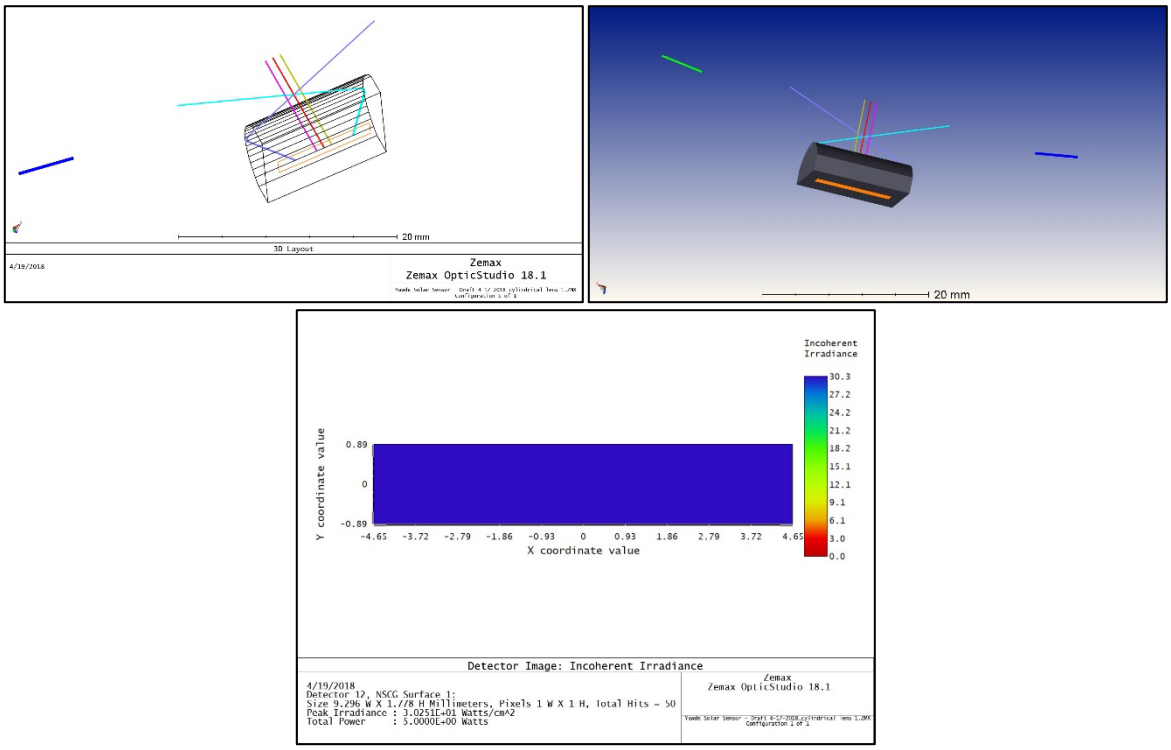

Note: 2-D model (top left), 3-D shaded model (top right), detector readout (bottom).

Figure 22
Cylindrical lens design and concept

The other consideration in this design is that the non-primary axis (rotational axis of the round) can be tailored to be the same width as the current assembly using masks or can be left open to allow a larger acceptance angle for more complex determination of the round's trajectory in respects to the sun and/or earth. Other considerations may apply to this concept such as increasing the machined placement slot located on the fuze nose itself but in a cheap, easily made rectangular shape with flat edges, above the photodiode region. Table 2 provides all the comparative detector readout values for each of the remodeled concepts that do not use the original slit housing and reflectors. Note these values are for all the incident angles.

Table 2
Detector readouts for the cylindrical lens, conical tube, and inverted cone conceptual designs.

	1x1 Photodiode detector	Emitter angle, all	
Sensor design	Incoherent irradiance, maximum (W/cm2)	Incoherent irradiance, nominal	Number of hits
Cylindrical lens	30.25	18.15	50
Conical tube	42.35	25.41	70
Inverted cone	18.15	10.89	30

Reflector and Assembly Redesign, Concept 5, Inverted Aluminum Cone

The fifth concept for applying a waveguide onto the existing photodiode and cup involved the removal of the current slit design assembly and placing an inverted aluminum cone over top of the detector plane. Figure 23 provides the conceptual design of the inverted cone. This initial design was thought to have some promise, but after moderate attempts, the 81.5 and 69-deg critical angles could not be directed in toward the detector plane. This is primarily a physical limit set by the long axis of the photodiode, the maximum internal tapered angle of the cone, and lights attribute of reflecting through a normal angle. Overall, this design does not have any significant viability given its initial results. See table 2 for detector readout comparisons to the other replacement designs not using the slit assembly.

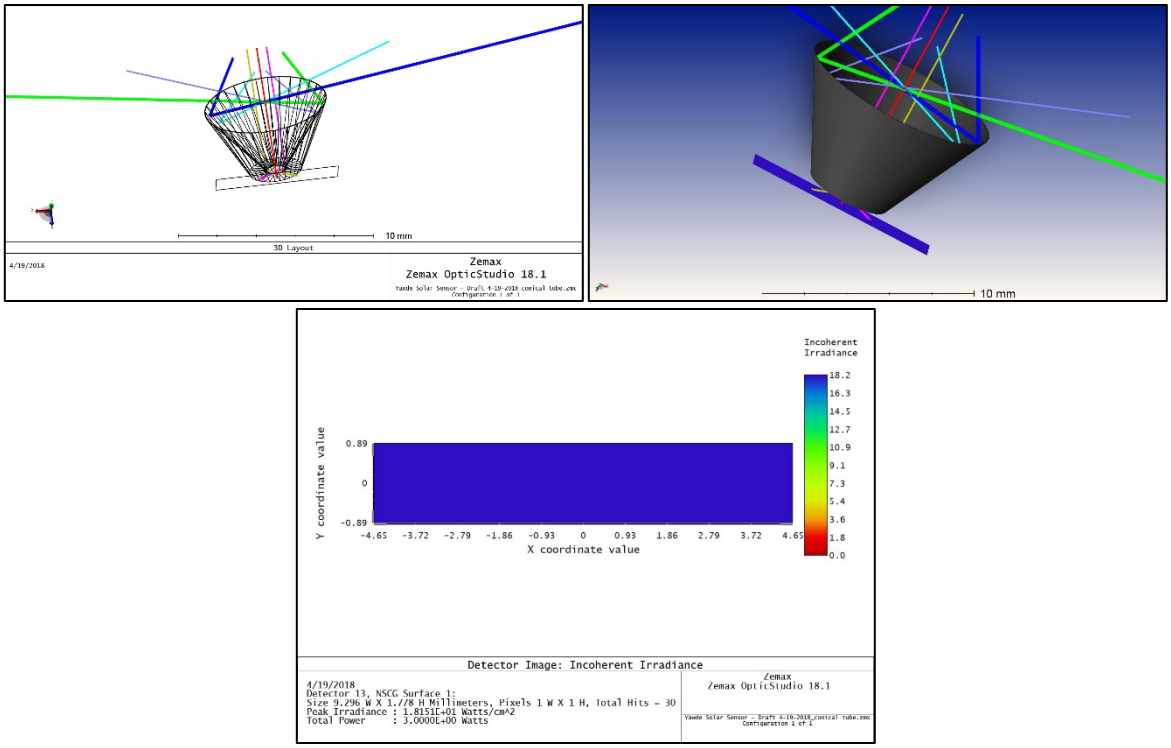

Note: 2D layout (top left), 3D shaded model (top right), and detector output (bottom).

Figure 23
Inverted aluminum cone

Reflector and Assembly Redesign, Concept 6, Conical Aluminum Cone

The sixth and final concept that was reviewed under this preliminary redesign of the solar sensor was the use of an aluminum conical shape. This design is essentially rotated 90-deg about the long axis of the inverted cone design. Figure 24 provides the illustration for this design, which shows that having the smaller aperture opening allows for the photons to enter the detector plane at all the critical angles and reflect downward. These conditions mimic the slit assembly in the long axis of the detector and also allow for additional compensation for the non-primary axis (short axis of the detector) if needed. This design can be easily masked to have the same width of the detector to also leave the non-primary axis the same under the current slit width. With this concept, the mounting can also increase efficiency by not needing the alignment and mounting pins within the optical cavity but by using a thick side wall, which can be milled/machined to allow fixturing to the fuze wall via a tap and die configuration. This would be done such that the outer cylinder surrounding the cone could screw into the fuze wall. The only other manufacturing consideration would be the photodiode mounting to the cone. An option here would be to machine an insert to the size of the photodiode/cup and use NOA-61 to adhere the two together while not impacting the optical properties of the design. Overall, this concept also reinforces potential in the tapered reflector slit design (option 2), excluding the fact that the physical dimensions of the photodiode is the inherent limiting factor as well as the size constraints provided. See table 2 for comparative results of the detector readout.

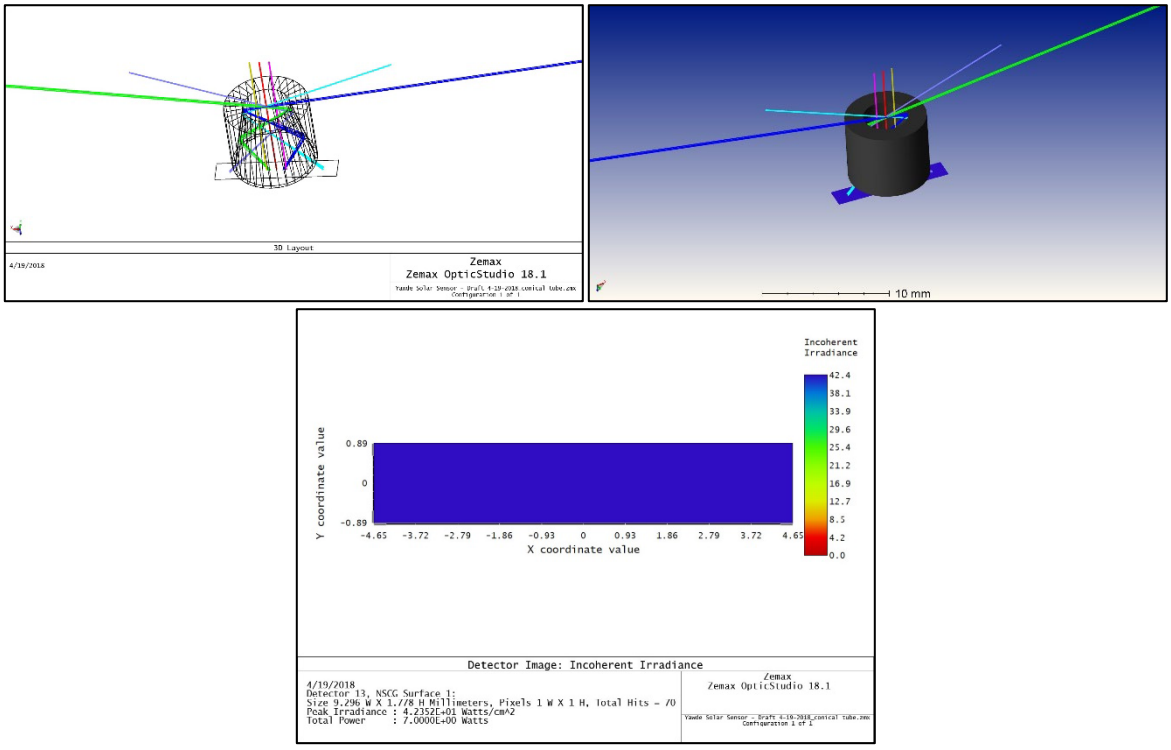

Note: 2-D layout (top left), 3-D shaded model (top right), and detector output (bottom).

Figure 24
Conical aluminum cone

Environmental Considerations

The linear temperature expansion coefficients (μm/mK) of brass is roughly 18 to 19, while aluminum is roughly 21 to 24, the stainless steel of the dowels/pins roughly 14 to 17.5, and nickel at 13 (ref. 8). This in comparison to N-BK-7 borosilicate glass at a coefficient of 7.1E-6 shows that any of the above concept should be able to handle the temperature loading of the fired projectile and stay intact as far as the assembly goes. The ability to handle the setback forces, however, will require a more thorough investigation into hardness and other material characteristics associated with shock and vibration to assure ruggedness and robustness. Long term storage does not appear to be a factor at this stage to discount any options on the basis of material other than the longevity of the optical adhesive under extreme conditions. This portion of design viability will require additional consideration to assure a fully compatible replacement that can handle the required conditions.

CONCLUSIONS

Overall, six options were reviewed to replace the current nickel plated brass slit reflector Yawsonde solar sensor. The options included replacing the reflector material with aluminum, two tapered designs on the reflectors to reduce machine/milling complexity on the current reflector, a full replacement using a glass cylindrical lens and optical adhesive, and two conical cone designs. The inverted cone showed the worst waveguide performance; the aluminum conical shape had the best performance. The cylindrical lens was comparable to the current design's performance except at the extreme angles, and the tapered designs appear at the top level to be possible but likely will increase the complexity of the design even more due to size restraints. All of the analysis assumed the photodiode was a single pixel detector, which in the modeling recorded either a hit or miss type of response. For each design, seven incident angles from the emitter were assessed which simulated the fuze and projectile traversing up to and after the apogee of the round. These angles were normal to the detector plane (0 deg) and normal just off-center in both positive and negative directions at +/-69 deg and at the critical angle of +/-81.5 deg. These angles are relative to the arc-distance of the sun as seen on earth.

To assure any of the options can be a complete replacement with cost savings, additional testing, more precise modeling, and additional research must be made. This initial assessment shows there is potential if a replacement is under full consideration. In the event additional resources are provided to continue this effort, a cooperative patentable design may be achieved complete with bottom up modeling, prototyping, and life-fire testing.

REFERENCES

1. Zemax LLC (2018). Zemax OpticStudio (version 18.1) [Software]

2. https://refractiveindex.info/?shelf=main&book=Al&page=Rakic.

3. Hepner, D. J., Hollis, M. J., Mitchell, C. E., "Yawsonde Technology for the Jet Propulsion Laboratory (JPL) Free Flying Magnetometer (FFM Program)" Technical Report ARL-TR-1610, Defense Technical Information Center, U.S. Army ARL, Aberdeen Proving Ground, MD, July 1998.

4. Feguson, E. M., Hepner, D. J., Clay, W. H., "Multisensor Pinhole Yawsonde" Technical Report ARL-TR-213, Defense Technical Information Center, U.S. Army ARL, Aberdeen Proving Ground, MD, September 1993.

5. Elmore, R. E., "HDL Yaw Sonde Instrumentation", Technical Report HDL-TM-71-19, Defense Technical Information Center, Harry Diamond Labs, Washington, D. C., September 1971.

6. Baroni, A. and Struck, J., "Yaw Sonde Capabilities" Laboratory Report (Unpublished), Commodity Evaluation Division Armament Engineering Directorate, U.S. ARDEC, Picatinny Arsenal, NJ.

7. Gutler, E. and Gibbons, J., "Short Intrusion Yaw Sonde Development And Test Program," Laboratory Report TSI-D 1-76 (Unpublished), Instrumentation Division Technical Support Directorate, U.S. Army ARDEC, Picatinny Arsenal, NJ, October 1976.

8. https://www.engineeringtoolbox.com/linear-expansion-coefficients-d_95.html.

LIST OF SYMBOLS, ABBREVIATIONS, AND ACRONYMS

ARDEC	U.S. Army Research, Development and Engineering Center
avg	average
c	centi-, 1E-2
C	Celsius
CAD	computer aided design
CCD	charge coupled device
DC	direct current
DEVCOM AC	U.S. Army Combat Capabilities Development Command Armaments Center
F	Fahrenheit
ft	feet
g	grams
in.	inch
ISO	International Standards Organization
k	kilo-, 1E3
M	Mega-, 1E6
m	meter
mil	artillery mil, 3.477 MOA
mm	millimeter, 1E-3
MOA	minutes of Arc, 0.2876 mils
n	nano-, 1E-9
NIR	near infrared
oz	ounces
Rad	radians
ROI	region of interest
RDECOM	Research Development and Engineering Command
SAFC	Smalls Arms Fire Control
SD	standard deviation
Si	Silicon
SN	serial number
µ	micro-, 1E-6
UUT	unit(s) under test
W	Watts
WSEC	Weapons Software and Engineering Center

DISTRIBUTION LIST

U.S. Army DEVCOM AC
ATTN: FCDD-ACE-K
FCDD-ACW-FN, S. C. Zuber
J. Hitscherich
A. Lansey
Picatinny Arsenal, NJ 07806-5000

Defense Technical Information Center (DTIC)
ATTN: Accessions Division
8725 John J. Kingman Road, Ste 0944
Fort Belvoir, VA 22060-6218

GIDEP Operations Center
P.O. Box 8000
Corona, CA 91718-8000
gidep@gidep.org

REVIEW AND APPROVAL OF ARDEC TECHNICAL REPORTS

Yawsonde Solar Sensor	
Title	Date received by LCSD
Stephan Zuber, James Hitscherich, Andrew Lassey	
Author/Project Engineer	Report number (to be assigned by LCSD)
X4130 95	RDAR-WSF-N
Extension Building	Author's/Project Engineers Office (Division, Laboratory, Symbol)

PART 1. **Must be signed before the report can be edited.**

a. The draft copy of this report has been reviewed for technical accuracy and is approved for editing.

b. Use Distribution Statement A_X_, B____, C____, D____, E____, F____ or X____ for the reason checked on the continuation of this form.

1. If Statement A is selected, the report will be released to the National Technical Information Service (NTIS) for sale to the general public. Only unclassified reports whose distribution is not limited or controlled in any way are released to NTIS.

2. If Statement B, C, D, E, F, or X is selected, the report will be released to the Defense Technical Information Center (DTIC) which will limit distribution according to the conditions indicated in the statement.

c. The distribution list for this report has been reviewed for accuracy and completeness.

Joshua Charm

Division Chief (Date)

PART 2. To be signed either when draft report is submitted or after review of reproduction copy.

This report is approved for publication.

Joshua Charm

Division Chief (Date)

SMCAR Form 49, 20 Dec 06 supersedes SMCAR Form 49, 1 Nov 94.